**RAA 2020** Vol. **20** No. **7**, 111(6pp) doi: 10.1088/1674–4527/20/7/111

*http://www.raa-journal.org* *http://iopscience.iop.org/raa*

***R**esearch in*
***A**stronomy and*
***A**strophysics*

# Pulsar timing observations with Haoping Radio Telescope

Jin-Tao Luo[1,2], Yu-Ping Gao[1,3], Ting-Gao Yang[1], Cheng-Shi Zhao[1], Ming-Lei Tong[1], Yong-Nan Rao[1,2], Yi-Feng Li[1,2], Bian Li[1], Xing-Zhi Zhu[1], Hai-Hua Qiao[1] and Xiao-Chun Lu[1,2]

[1] National Time Service Center, Chinese Academy of Sciences, Xi'an 710600, China; *jluo@ntsc.ac.cn*
[2] Key Lab of Precision Navigation & Timing Technology, Chinese Academy of Sciences, Xi'an 710600, China
[3] University of Chinese Academy of Sciences, Beijing 100049, China

Received 2020 January 10; accepted 2020 March 5

**Abstract** We report pulsar timing observations carried out in $L$-band with NTSC's 40-meter Haoping Radio Telescope (HRT), which was constructed in 2014. These observations were carried out using the pulsar machine we developed. Timing observations toward millisecond pulsar J0437–4715 obtain a timing residual (r.m.s.) of 397 ns in the time span of 284 days. Our observations successfully detected Crab pulsar's glitch that happened on 2019 July 23.

**Key words:** radio telescopes — instrumentation: miscellaneous — methods: data analysis — pulsars: general

## 1 INTRODUCTION

The 40-meter Haoping Radio Telescope (HRT), operated by the National Time Service Center (NTSC), is a new radio astronomy facility in China. HRT is located in the Qinling mountains, ∼100 km east of the city of Xi'an.

As a national unit for scientific research, NTSC is an institute dedicated to carrying out professional research on time and frequency sciences. Among NTSC's research areas, the pulsar time plays an important role. At NTSC, the pulsar timescale, the assemble pulsar timescale, and the application of pulsar timescale have been well studied (Yang 2003; Yin et al. 2016; Tong et al. 2017). These studies are mainly on the theory and algorithms, using the data from PTAs (Pulsar Timing Arrays), such as Parkes Pulsar Timing Array (PPTA) in Australia, which are outside of China. With the construction of HRT and the development of a pulsar machine, NTSC started pulsar timing observations from the year of 2018.

This paper will present an introduction to the 40-meter HRT and the pulsar machine developed for this telescope. The pulsar timing observations taken with this system and the latest timing results will also be reported, including millisecond pulsar timing and glitch monitoring.

**Table 1** Some Key Specifications and Performances of HRT

| Spec/Para | Value |
|---|---|
| AZ range | $\pm$ 320° |
| EL range | 5° ∼ 92° |
| Max. AZ Speed | 1.5° s$^{-1}$ |
| Max. EL Speed | 1° s$^{-1}$ |
| Min. Speed | 0.0005° s$^{-1}$ |
| Pointing Accuracy | ≦1/10 Beam Width |

## 2 PULSAR TIMING OBSERVING SYSTEM

### 2.1 Radio Telescope

The HRT was constructed in 2014. As shown in Figure 1, the site is located deep in the mountains. Benefits from the isolation from cities and the protection of surrounding small hills, the site is a very good radio environment. However the nearby hills do not cause serious blockage to the telescope. Objects with elevation angles larger than 7° are visible to the telescope.

As shown in Figure 2 the telescope is a Cassegrain antenna system. The main reflector, which consists of full solid panels, is installed on an altitude-azimuth mount. The surface accuracies (r.m.s.) of the main and secondary reflectors are ≦0.6 mm and ≦0.15 mm, respectively. Table 1 lists some key specifications and performances of the telescope.

**Fig. 1** The bird view of 40-meter Haoping Radio Telescope.

**Fig. 2** The close view of 40-meter Haoping Radio Telescope.

### 2.2 Receivers

HRT is equipped with $L$-band and $S$-band receivers. The horns of these receivers can be seen in Figure 2. The $L$-band receiver, which is used to carry out pulsar observations, covers the frequency range of 1.1∼1.75 GHz. Before November 2019, we conducted single-polarization observations with HRT as only the RCP (Right Circular Polarization) was received. Since then, with the installation of the LCP (Left Circular Polarization) receiving system, both two polarizations are available. As shown in Figure 3, the RCP and LCP RF (Radio Frequency) signals, are amplified using the room-temperature LNAs (Low Noise Amplifiers) in the cabin and then transferred to the control room via the fiber using the RF-over-Fiber technology.

At the control room the RF signals are down converted using the LO (Local Oscillator) frequency of 1 GHz, producing IF (Intermediate Frequency) signals with the bandwidth of 800 MHz. The properly-amplified IF signals are then sent to the pulsar machine for further processes.

The system temperature of the $L$-band receiving system is about 100 K.

### 2.3 Pulsar Machine

IF signals from the receiving system are processed in the pulsar machine, such a backend development uses the FPGA+GPU architecture at HRT. Table 2 lists some key specifications of the machine.

As shown in Figure 3 IF signals are first digitized using the high speed ADCs (Analog-to-Digital Converters), whose sampling clock rates can be adjusted to meet the observing requirement. Digital IF signals then get processed on the FPGA (Field Programmable Gate Array) platform, which is based on the ROACH2 board developed by University of California (UC), Berkeley in the project of CASPER (Hickish et al. 2016). On the FPGA the digital IF signals first get divided into sub-channels using filter banks. In the coherent dedispersion mode the baseband data of these channels are directly sent out. In the incoherent dedispersion mode the calculation of four Stokes parameters, and the following process of accumulation which aims to reduce the data rate, are applied to each sub-channel.

The output of the FPGA is transferred to a 8-node GPU (Graphics Processing Unit) cluster via one 10 GbE (10 Giga bit Ethernet) interface in the incoherent dedispersion mode, and via eight 10 GbE interfaces in the coherent

dedispersion mode. In the incoherent mode the output data is processed on one node of the cluster. Depending on the observation type, the machine stores the search mode raw data directly or folds the data using a given ephemeris file and then stores the sub-integration profiles into the storage. The stored data is in the PSRFITS format. Similar operations are implemented on the eight nodes of the cluster in the coherent mode, while each node processes one eighth of the total observing band. The pulsar machine is controlled using a computer through the 1 GbE (1 Giga bit Ethernet) links.

The 10 MHz signal from the on-site Cesium atomic clock is used to generate input clocks for ADCs. This clock's 1 PPS (Pulse Per Second) signal is used to trigger the pulsar machine. Additionally this atomic clock is synchronized to UTC (NTSC) with an error less than 2 ns using the satellite CV (Common View) technique. These ensure precise and stable time and frequency signals, together with an accurate on-site time reference for pulsar timing observations.

PSR J1939+2134, a millisecond pulsar with a period of $\sim$1.56 ms, is used to test the coherent dedispersion functionality. The coherent dedispersion technology can recover the true pulse shape of this pulsar (McMahon 2008). Figure 4 shows the integrated profile of PSR J1939+2134 obtained with our pulsar machine in coherent dedispersion mode. As shown in this figure the fine structure of this pulsar's main pulse, around phase 0.75, was recovered.

## 3 MILLISECOND PULSAR TIMING

### 3.1 Observation

The long-term millisecond pulsar timing observing program started from the end of August 2018. Several millisecond pulsars are being regularly observed with cadences ranging from $\sim$3 days to 1 month. The brief parameters and observing configurations of these millisecond pulsars are listed in Table 3.

Before August 2019, observations were carried out in the incoherent dedispersion mode, and since then observations were taken using the coherent dedispersion mode. In both modes 1024-channel mode were used, together with 1024 phase bins. The length of the sub-integration is set to 10 seconds, in order to keep a good time resolution for the detection and mitigation of time-domain burst interferences in the data process. For observations in the incoherent mode, the time resolution is set to 10.24 μs.

These observations use the ephemeris from PSRCAT[1] (Manchester et al. 2005) and NANOGrav (Arzoumanian et al. 2018) and PPTA[2] (Reardon et al. 2016).

### 3.2 Data Reduction and Analysis

The data reduction and analysis is implemented using the pulsar software `PSRCHIVE` (Hotan et al. 2004). The raw data, which store sub-integration profiles, first get updated with ephemeris released from PPTA and (or) NANOGrav using the program `PAM`. Then the program `PAZI` is used to do manual RFI mitigation. No calibration is applied as HRT has not been equipped with flux and polarization calibration capability.

TOAs (Time Of Arrivals) are generated with the program of `PAT`, using profiles released from PPTA and NANOGrav as the template. Timing analysis is then carried out using the software `TEMPO2` (Hobbs et al. 2006).

### 3.3 Results

We take J0437–4715 as the example of our millisecond pulsar observations. Its integrated profile is shown in Figure 5. With an integration time of $\sim$75 minutes, the profile obtained with our system shows an SNR of $\sim$640.

Figure 6 shows the timing residual of PSR J0437–4715. In the time span of 284 days, the obtained timing residual (r.m.s.) is 397 ns. As can be seen in this figure, the distribution of TOA dots are not random which suggests there are system errors that need to be removed. The lack of polarization calibration is a likely cause of these errors.

## 4 GLITCH MONITORING

### 4.1 Observation

A few pulsars which have glitch records are being monitored via timing observations at HRT. Configurations of these observations are the same as introduced in Section 3.1. With these observations we managed to detect the Crab pulsar's glitch event that happened on 2019 July 23. In timing observations towards the Crab pulsar (PSR J0534+2200) the ephemeris from PSRCAT is used and the observing length varies from $\sim$20 minutes to 2 hours.

### 4.2 Data Reduction and Analysis

The process is the same as that introduced in Section 3.2. For the Crab pulsar, the monthly ephemeris released by

[1] *http://www.atnf.csiro.au/research/pulsar/psrcat*

[2] *https://data.csiro.au/collections/#collection/CIcsiro:13081v3*

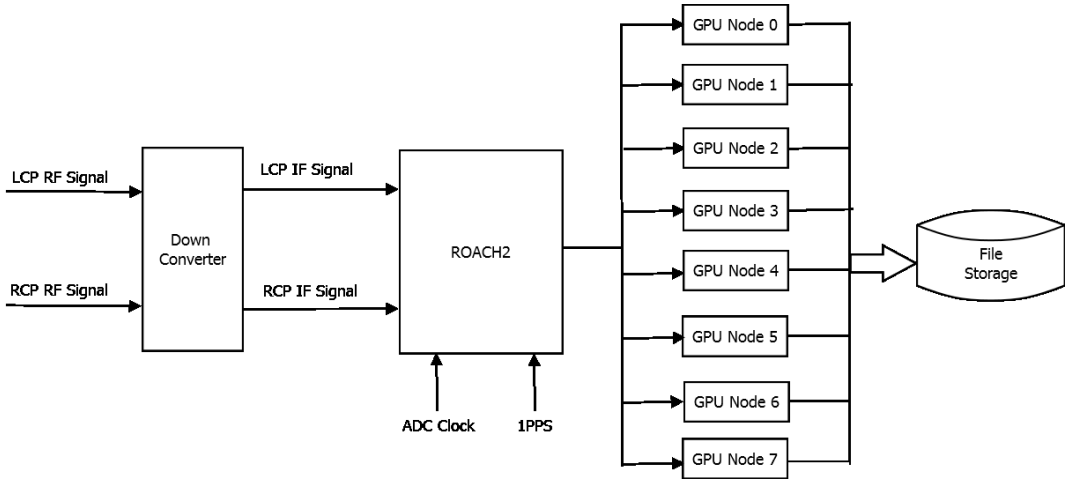


**Fig. 3** Diagram of the Pulsar Timing System.

**Table 2** Specifications of Pulsar Machine at HRT

| | |
|---|---|
| Incoherent Dedispersion Mode | |
| Obs. Mode | Fold, Search |
| Maxi. Bandwidth | 2 GHz |
| No. of Channels | 8192, 4096, 2048, 1024, 512, 256, 128, 64 |
| Highest Time Resolution | 10.24 μs |
| Coherent Dedispersion Mode | |
| Obs. Mode | Fold, Search |
| Maxi. Bandwidth | 1.6 GHz |
| No. of Channels | 4096, 2048, 1024, 512, 256, 128, 64 |
| Highest Time Resolution | $<$ 10.24 μs |

**Table 3** Brief Parameters and Observing Configurations of Millisecond Pulsars

| Pulsar Name | RaJ (h:m:s) | DecJ (d:m:s) | Period (ms) | DM ($cm^{-3}$ pc) | Obs. Cadence | Obs. Length |
|---|---|---|---|---|---|---|
| J0437–4715 | 04:37:15.90 | −47:15:09.11 | 5.757 | 2.64476 | ∼3 days | $>$ 40 min |
| J1713+0747 | 17:13:49.53 | +07:47:37.48 | 4.570 | 15.917 | ∼3 weeks | $>$ 40 min |
| J1939+2134 | 19:39:38.56 | +21:34:59.13 | 1.558 | 71.0237 | ∼1 month | $>$ 40 min |
| J1909–3744 | 19:09:47.43 | −37:44:14.46 | 2.947 | 10.3932 | ∼1 month | $>$ 40 min |
| J1022+1001 | 10:22:57.99 | +10:01:52.77 | 1.645 | 10.2521 | ∼1 month | $>$ 40 min |
| J1643–1224 | 16:43:38.16 | −12:24:58.68 | 4622 | 62.4143 | ∼1 month | $>$ 40 min |
| J2145–0750 | 21:45:50.46 | −07:50:18.51 | 1.605 | 8.99761 | ∼1 month | $>$ 40 min |

Jodrel Bank Observatory[3] (Lyne et al. 1993) is used to update the data obtained with HRT. A high-quality profile obtained from our observations is used as the template.

According to the glitch catalog (Espinoza et al. 2011)[4], in the course of our observations the Crab pulsar had two glitch events which were reported to have happened on 2018 December 18 and 2019 July 23. In this paper we report the analysis on the latter one. TOAs from January to July in 2019 (before the event) are fitted to determine parameters before the glitch. This pre-glitch ephemeris is then used in the timing process on all the TOAs from January 2019, including TOAs before and after the July glitch event.

[3] `http://www.jb.man.ac.uk/~pulsar/crab.html`

[4] `http://www.jb.man.ac.uk/pulsar/glitches/gTable.html`

### 4.3 Results

Figure 7 shows an integrated profile of the Crab pulsar obtained from our observations. The integration time is ∼47 minutes, and the profile's SNR is ∼44. This profile clearly shows Crab pulsar's main pulse and interpulse, around phase 0.3 and 0.7 respectively. In this figure the precursor which is ∼0.1 phase before the main pulse (Lyne et al. 2013) can be seen as well.

The timing residual relative to the pre-glitch timing model is shown in Figure 8. The corresponding observations cover the period from MJD 58534 to MJD 58825. This residual shows an offset-and-return structure, which is typical in Crab pulsar's glitch timing residuals (Wang et al. 2001). Using the last pre-glitch data and the first post-glitch data in our observations, the estimated glitch

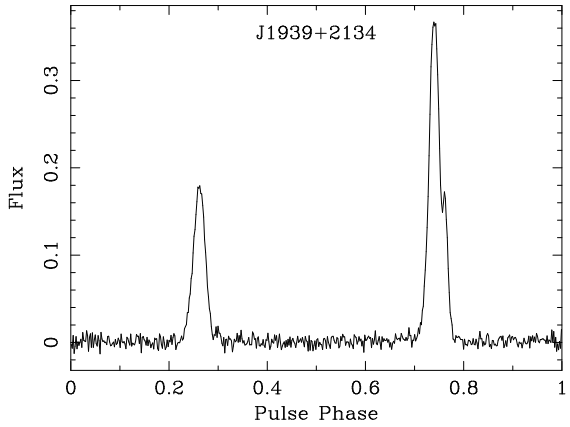


**Fig. 4** The integrated profile of PSR J1939+2134. The flux density is plotted in arbitrary units.

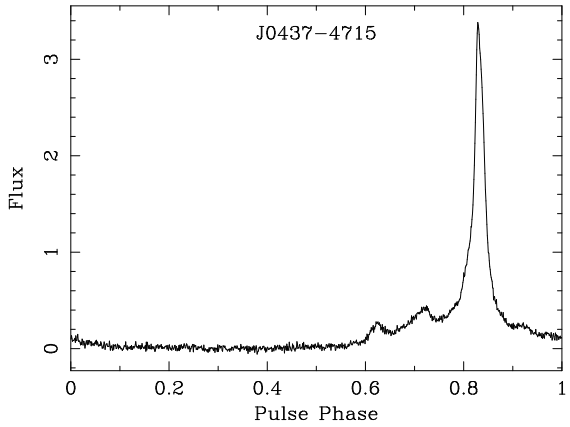


**Fig. 5** The integrated profile of PSR J0437–4715. The flux density is plotted in arbitrary units.

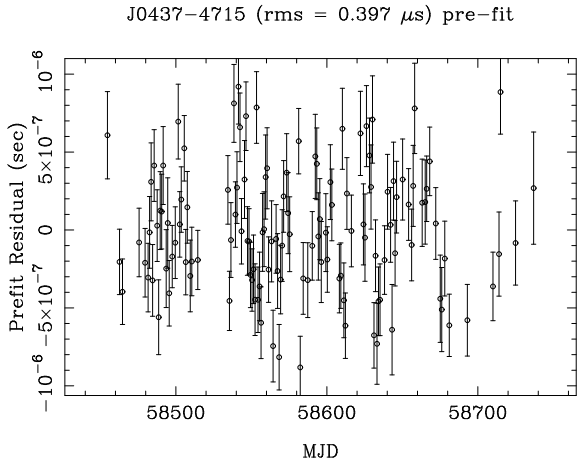


**Fig. 6** Timing residual (r.m.s.) of PSR J0437–4715.

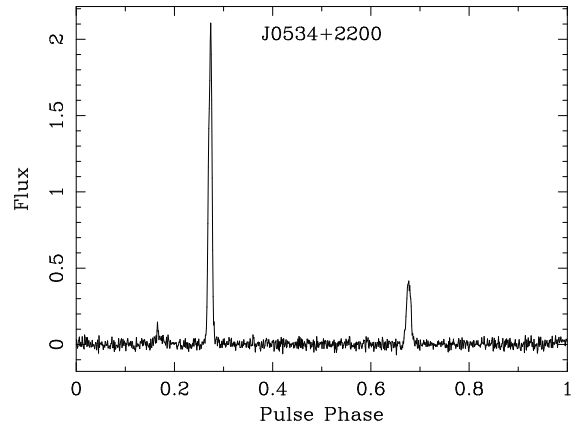


**Fig. 7** The integrated profile of the Crab pulsar. The flux density is plotted in arbitrary units.

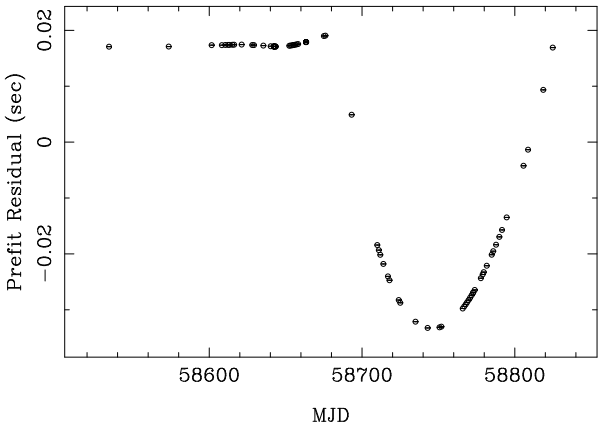


**Fig. 8** The timing residual of the Crab pulsar from MJD 58534 to MJD 58825.

epoch is MJD 58684.621 with the uncertainty of 8.584 days. The glitch epoch reported from the glitch catalog is MJD 58687.59. Our detection coincides with the report. The post-glitch TOAs show obvious offsets from the pre-glitch model and begin to return to this model from $\sim$ MJD 58750.

## 5 SUMMARY

We have developed a pulsar timing observing system at our 40-meter radio telescope. Using this system several millisecond pulsars and glitch pulsars are being observed. Timing observations toward millisecond pulsar J0437–4715 obtained a timing residual (r.m.s.) of 397 ns in the time span of 284 days. Timing observations toward the Crab pulsar, J0534+2200, has successfully detected this pulsar's glitch in July 2019. High-quality profiles of these two pulsars obtained with our system, together with the good timing residual on millisecond pulsar J0437–4715 and the detection of Crab pulsar's glitch, indicate that this system has a very good receiving sensitivity and system stability for pulsar timing observations.

After installing the receiving system for the LCP signal, we are working on the calibration capability of our

pulsar timing system. This effort is expected to improve the timing result of millisecond pulsars like J0437–4715.

**Acknowledgements** This work was supported by the Hundred Talents Program of the Chinese Academy of Sciences (Technological excellence, Y650YC1201), the National Natural Science Foundation of China (Grant Nos. U1931128, 11973046, 91736207, U1831130, 11903038, 11873050 and 11873049). The Natural Science Foundation of Shaanxi Province (Grant No. 2019JM-455), and the program of Youth Innovation Promotion Association CAS (2017450).

## References

Arzoumanian, Z., Brazier, A., Burke-Spolaor, S., et al. 2018, ApJS, 235, 37

Espinoza, C. M., Lyne, A. G., Stappers, B. W., & Kramer, M. 2011, MNRAS, 414, 1679

Hickish, J., Abdurashidova, Z., Ali, Z., et al. 2016, Journal of Astronomical Instrumentation, 5, 1641001

Hobbs, G. B., Edwards, R. T., & Manchester, R. N. 2006, MNRAS, 369, 655

Hotan, A. W., van Straten, W., & Manchester, R. N. 2004, PASA, 21, 302

Lyne, A. G., Pritchard, R. S., & Graham Smith, F. 1993, MNRAS, 265, 1003

Lyne, A., Graham-Smith, F., Weltevrede, P., et al. 2013, Science, 342, 598

Manchester, R. N., Hobbs, G. B., Teoh, A., & Hobbs, M. 2005, AJ, 129, 1993

McMahon, P. 2008, Adventures in Radio Astronomy Instrumentation and Signal Processing, 18 (Univ. of Cape Town), *http://www.rrsg.uct.ac.za/theses/msc_theses/pmcmahon_thesis.pdf*

Tong, M. L., Yang, T. G., Zhao, C. S., & Gao, Y. P. 2017, Scientia Sinica Physica, Mechanica & Astronomica, 47, 099503

Reardon, D. J., Hobbs, G., Coles, W., et al. 2016, MNRAS, 455, 1751

Wang, N., Wu, X.-J., Manchester, R. N., et al. 2001, ChJAA (Chin. J. Astron. Astrophys.), 1, 195

Yang, T.-G. 2003, Journal of Time and Frequency, 26, 25

Yin, D. S., Gao, Y. P., & Zhao, S. H. 2016, Acta Astronomica Sinica, 57, 326